



**ASSESSMENT OF THE PROMPT RADIATION HAZARDS OF TRAPPED
ANTIPROTONS**

J. Donald Cossairt^{*}

Abstract - Investigators at several laboratories are seriously considering the storage and transport, perhaps over long distances, of very low energy antiprotons as a part of basic physics research programs and perhaps even for practical applications. To do this will require proper attention to the prompt radiation hazards due to the release of energy in the annihilations of antiprotons with nucleons, under either planned or accidental circumstances. In this paper, a simple model is used to describe the radiation field. Elementary shielding calculations for a simple source of annihilating antiprotons are presented. It is concluded that these radiation fields are readily understood and that the radiation hazards can be mitigated using conventional means.

Key words: dose assessment, antiprotons, pions, photons, shielding, dose equivalent

^{*}Fermi National Accelerator Laboratory, P. O. Box 500, Batavia, IL 60510. Email:
cossairt@fnal.gov.

INTRODUCTION

The antiproton, the antiparticle of the ordinary proton, has now been studied for over 40 years (Eades and Hartmann 1999). Over the last two decades, a number of investigators have speculated on the possibility that these particles can be stored at low kinetic energy and perhaps even transported. Antiprotons of relatively high energies have been copiously produced at the proton accelerators at both the European Organization for Nuclear Research (CERN) in Geneva, Switzerland and the Fermi National Accelerator Laboratory (Fermilab) in Batavia, IL, USA using proton-nucleus reactions at high energies. At both of these laboratories, the principal disposition of these particles has been their collection in storage rings followed by their subsequent acceleration to high energies for collision with protons in particle physics experiments conducted at frontier energies on the scale of 10^{12} electron volts (TeV). Other important basic research studies with antiprotons have been conducted at more modest energies, for example, the body of work performed at the low-energy antiproton ring (LEAR) at CERN, where antiprotons having low momenta are acquired by decelerating higher energy antiprotons. Review articles by Amsler and Myhrer (1991), Landau (1996), and Amsler (1998) provide useful summaries.

Since their invention in 1936, Penning traps have been used to store electrons, charged particles, and ions by means of special configurations of magnetic and electric fields. Brown and Gabrielse (1986) have described these devices at length. Obviously, the trapping of antiprotons involves considerable technological challenges since the particles have to be produced, collected and then stored. Antiprotons have been successfully captured in a Penning trap at very low energies at LEAR (Gabrielse et al. 1986). In this experiment, about 300 antiprotons were captured and it was concluded that confinement of perhaps 30,000 or so for time periods as long as 10 months is feasible. Currently, considerable effort is directed toward eventually studying

cold antihydrogen in the laboratory (Gabrielse 2002). Howe, Hynes, and Picklesimer (1988) have investigated the research possibilities resulting from the ability to transport trapped antiprotons to locations distant from the large accelerators where they can be produced. The feasibility of the transport of as many as 10^{12} antiprotons in this manner was considered. The possibility of long distance transport has been demonstrated, in principle, by the successful shipment of electrons from California to Massachusetts in a Penning trap using a motor vehicle on highways (Tseng and Gabrielse 1993). Indicative of the near-term possibilities, this was achieved without connection to electrical power by using the persistent field of a superconducting magnet along with electric fields produced with 9 Volt batteries.

Along with the obvious benefits to particle and nuclear physics, having antiprotons “readily available” at energies near rest in the laboratory frame of reference could be useful to the fields of atomic and condensed matter physics. There are also ideas that stored antiprotons might be useful as a compact source of stored energy, perhaps in medicine or in spaceflight. Thus, it behooves members of the radiation protection profession to understand further the associated radiological hazards in order to assist in the beneficial utilization of these particles. This topic has received little study since most interest in antiprotons has occurred at the high energy physics laboratories where they are produced. There, the radiation protection concerns involved with the proton-nucleus collisions used to produce the antiprotons generally dominate over those due to the annihilating antiprotons.

METHODS

Radiation field produced by proton-antiproton annihilations

In this paper, those aspects of the radiation field emitted by antiproton-nucleon

annihilations occurring at rest in the laboratory frame of reference that are important for radiation protection purposes will be emphasized, with the production of exotic particles and measurement of rare processes left to particle physics. At low energies near rest, the process of interest is solely that of annihilation. Pais (1960) employed group-theoretical techniques to describe the properties of systems of specific numbers of pions, working out various quantum numbers and branching ratios that are suitable for further use. The results were specifically applied to antiproton-nucleon annihilations and recognized that, "...the average number of π -mesons produced in \bar{p} -annihilation is about 5 or 6." Both charged (π^\pm) and neutral (π^0) pions are emitted from these events. Momentum conservation requires the emission of at least two particles from each annihilation event. Amsler (1998), in an up-to-date review paper, reported that average multiplicities in annihilations at rest in the laboratory frame of reference are 3.0 ± 0.2 for charged pions and 2.0 ± 0.2 for neutral pions. Further, the numbers of pions are distributed statistically as a Gaussian function about these mean values, with a standard deviation of about one. The statistical model of antiproton annihilations has been called "the fireball model". There are other particles produced aside from pions, the most prominent being the η -meson (rest energy of 547.3 MeV) in 7% of annihilations and the K-meson (rest energy of 493.7 MeV) in about 6%. These and other "rare process" particles will not be given further consideration here. All particle rest energies and mean lives are those of the Particle Data Group (Groom et al. 2000).

One can proceed to develop appropriate energy spectra from a simple statistical mechanical point of view, constrained to be consistent with the above results. In an annihilation event where both a proton and an antiproton are at rest, the total energy available is twice the rest energy of the proton, a total of 1876.5 MeV. Assuming that at the instant of annihilation, this

energy is shared equally (i.e., equipartitioned) among the average five pions, the mean of the total energy awarded to each would be 375.3 MeV. A charged pion has a rest energy of 139.6 MeV, therefore, each charged pion has an average kinetic energy, $\langle E_{\pi^{\pm}} \rangle = 235.7$ MeV. The situation is somewhat different for the neutral pions. The mean life of the π^0 is extremely short, only 8.4×10^{-17} s. Therefore, at their mean kinetic energy, these particles travel only an average distance of 65.1 nm before decaying. The most prominent decay branch, by far, (98.8 %) is into two photons. Thus, each photon is awarded a mean energy, $\langle E_{\gamma} \rangle = 187.6$ MeV. It follows there are an average of four such photons emitted in each annihilation. Thus the radiation field is comprised of two components, an electromagnetic part due to the photons from the neutral pions and a hadronic part due to the charged pions.

Since the pions as well as the decay photons have integer spin, they are classified as *bosons* and hence their “natural” statistical mechanical distribution is the Bose-Einstein function, which for the massless photons can be expressed as follows:

$$N_{\gamma}(E_{\gamma}) = \frac{C_{\gamma} E_{\gamma}^2}{\exp(E_{\gamma}/kT_{\gamma}) - 1}. \quad (1)$$

$N_{\gamma}(E_{\gamma})$ is the number of photons having energy E_{γ} per unit energy and the product, kT_{γ} , represents the product of Boltzmann’s constant and the absolute “temperature”, in a statistical mechanical picture (for example, Tolman 1938). The product, kT_{γ} , is conventionally expressed in MeV. In this work, a spectrum spanning the energy range from 0 up to 938 MeV was generated using this function. A value of kT_{γ} of 69.5 MeV was found to result in a spectrum for which the average value of E_{γ} matched that calculated above while the value of C_{γ} was set to 1.242×10^{-6} MeV⁻³ to achieve the average yield of 4.0 photons per annihilation for the numerical integration of $N_{\gamma}(E_{\gamma})$.

over the spectrum. This spectrum is similar in shape to that employed by Howe et al. (1988). Others have reported the use of a Monte Carlo generated spectrum for these photons in order to subtract backgrounds in physics experiments (e.g., Graf et al. 1991). One also needs dose equivalent per fluence conversion factors, $P_\gamma(E_\gamma)$. The *maximum* values tabulated by Fasso et al. (1990) are used and are displayed in Fig. 1 along with the energy spectra.

A spectrum for the charged pions was generated in similar fashion using the Bose-Einstein distribution. For these particles of non-zero rest mass, this takes the more general form:

$$N_\pi(E_\pi) = \frac{C_\pi p_\pi W_\pi}{\exp(W_\pi / kT_\pi) - 1}. \quad (2)$$

$N_\pi(E_\pi)$ is the number of charged pions of either sign having kinetic energy E_π per unit energy, p_π is the momentum, and W_π is the total relativistic energy given by $E_\pi + m_\pi$, with m_π denoting the rest energy of the charged pion. The relativistic form is needed since the kinetic energies of the pions are comparable with their rest energy. As for the photons, a spectrum was generated according to this function spanning the energy domain from 0 to 938 MeV. The value of C_π was set to $4.998 \times 10^{-7} \text{ MeV}^{-3}$ to normalize the integral of this expression over energy to the yield of 3.0 charged pions per annihilation while a value of kT_π of 110.0 MeV was found to reproduce the average charged pion kinetic energy found above[†]. Reported experimental energy or momentum spectra for these charged pions are fragmentary at best. These have largely been measured for background subtraction purposes in experiments studying rare processes and commonly appear to reflect significant instrumental threshold effects. In Fig. 2, two examples of measured spectra (Gregory et al. 1976) and Angelopoulos et al. 1986) are compared with the spectrum calculated using eqn (2). It is concluded that the spectrum generated by eqn (2) is sufficiently representative for radiation protection purposes. It is also similar in shape to that used by Howe et al. (1988).

As with the photons, one needs dose equivalent per fluence conversion factors, $P_{\pi}(E_{\pi})$, for charged pions. These were taken from Fasso et al. (1990). Since at low energies the values of $P_{\pi}(E_{\pi})$ for positive pions are smaller than those for negative pions, the averages for the two charge states were used for energies below 60 MeV. Above that level, the results of Stevenson (1986) (also listed by Fasso et al. 1990) were employed. The results are included in Fig. 2.

Radiation field for a “bare” Penning Trap

If antiprotons are stored in a Penning trap or similar device for a long period of time (e.g., months), appreciable annihilations cannot occur on an ongoing basis without depleting the inventory. Thus, the intensity of steady-state prompt radiation near such a device will be at or near zero. Any prompt radiation is a result of a planned or unplanned event that terminates the storage. Terminating mechanisms, either accidental or intentional, are the loss or modification of the magnetic field perhaps due to the loss of electrical power or the failure of the cooling of a superconducting magnet, the collapse or alteration of the necessary electric field, or a failure of the vacuum in the device. Thus, the radiation is emitted in a nearly instantaneous "accident" and the hazard is that of the total acute dose equivalent. Recognizing the modest dimensions of practical Penning traps (see references), an isotropic point source approximation is reasonable, and one may choose to neglect any self-shielding of the materials comprising the trap. For an unshielded device, one only has to perform the following integrations, most readily done numerically, to get the dose equivalent per annihilation due to the photons, $H_{\gamma}(r)$ (Sv) and the dose equivalent per annihilation due to the charged pions, $H_{\pi}(r)$ (Sv):

$$H_{\gamma}(r) = \frac{1}{4\pi} \int_0^{938} \frac{dE_{\gamma} N_{\gamma}(E_{\gamma}) P_{\gamma}(E_{\gamma})}{r^2} = \frac{6.17 \times 10^{-11}}{r^2} \quad (3)$$

and

$$H_{\pi}(r) = \frac{1}{4\pi} \frac{\int_0^{938} dE_{\pi} N_{\pi}(E_{\pi}) P_{\pi}(E_{\pi})}{r^2} = \frac{3.93 \times 10^{-10}}{r^2}, \quad (4)$$

where r (cm) is the distance from the source. The sum of $H_{\gamma}(r)$ (“electromagnetic component”) and $H_{\pi}(r)$ (“hadronic component”) is the total dose equivalent per annihilation, $H(r)$ (Sv).

Shielding of the electromagnetic component

Six shielding materials were studied; carbon, aluminum, iron, copper, lead, and concrete. “Concrete” is taken to be the mixture of elements specified by Chilton, Shultis, and Faw (1984) as “ordinary” concrete, with an average atomic number of 11.58 and an average mass number of 23.31. To shield the photons, one needs the photon mean free paths, λ_{γ} , for the shielding materials. The database of Berger, et al. (2002) was used to provide the values plotted in Fig. 3 for representative examples of possible shielding materials. To proceed further with the shielding of the electromagnetic component, pair production and the subsequent generation of electromagnetic cascades must be considered. This *radiative* component is characterized by other material-dependent parameters. Along with the density, ρ , these are the radiation length, X_o , and the critical energy, E_{crit} . X_o is the mean free path of radiative energy loss of electrons in matter independent of collisional stopping while E_{crit} is the energy above which more than half of the energy loss of an electron is radiative rather than collisional. For the present study, standard values of ρ were used, while those taken for X_o and E_{crit} follow the suggestions of Groom et al. (2000). The material-dependent parameter values are provided in Table 1.

Given the relatively weak energy dependence of the value of λ_{γ} over the relevant energy domain, the method employed to calculate the effects of shielding on the electromagnetic

component of the radiation field was to extensively utilize averages over this energy region weighted by the photon energy spectrum, $N_\gamma(E_\gamma)$. The spectrum-weighted average values for the photon mean free path, $\langle\lambda_\gamma\rangle$, were calculated for each material. The next step was to determine the spectrum-weighted average for the fraction of the total photon cross section that results in pair production. At each energy this fraction was obtained from Berger et al. (2002). From these data, the spectrum-weighted average of this fraction, F_{pair} , was found for each material. In a pair production event at the mean photon energy, $\langle E_\gamma \rangle$, of 187.6 MeV, Berger and Seltzer (1964) and Swanson (1979) have provided estimates of the fraction of the electrons at half this energy that will initiate an electromagnetic shower, F_{shower} . The product of F_{pair} and F_{shower} , F_{em} , is used here to estimate the fraction of the photons emitted by an annihilation that will initiate an electromagnetic cascade. In the present calculation, these values are conservative, since following the first generation of the electromagnetic shower, the energies of the electrons and positrons involved will be reduced, with reduced values of F_{pair} and F_{shower} .

Fasso et al. (1990) as well as Swanson (1979) present useful summaries of results from the so-called "Approximation B" of analytical shower theory, originally developed by Rossi and Griessen (1941). One needs the location of the shower maximum in the shield, the position of the maximum number of electrons and maximum energy deposition. For photon-initiated showers, the shower maximum is at a depth d_{shower} in the shield given by

$$d_{shower} = 1.01X_o \ln \left[\frac{\langle E_\gamma \rangle}{E_{crit}} \right] - 0.5, \quad (5)$$

where the average photon energy, $\langle E_\gamma \rangle$, is used. A Gaussian approximation can describe the spread of the shower away from its maximum by a root mean square distance, τ , given by

$$\tau = X_o \sqrt{\left\{ 1.61 \ln \left[\frac{\langle E_\gamma \rangle}{E_{crit}} \right] + 0.9 \right\}}. \quad (6)$$

Likewise the maximum energy deposited per radiation length, X_o , for a photon-induced shower is given by

$$D_{max} = \frac{0.31 F_{em} \langle E_\gamma \rangle}{\sqrt{\left[\ln \left(\frac{\langle E_\gamma \rangle}{E_{crit}} \right) - 0.18 \right]}}. \quad (7)$$

With unit conversions, the value of D_{max} can be transformed into the absorbed dose in the shielding material assuming isotropic emission from a point source. Finally, this absorbed dose in the shielding material must be converted to personnel dose equivalent with the help of a conversion factor, C_{mat} (Sv Gy⁻¹), provided by Fasso et al. (1990). The material-dependent shower parameters are given in Table 2.

At each depth, d , the above formalism was used to calculate the additional dose equivalent due to the electromagnetic cascade process. This was done for a point source surrounded by a spherical shield of thickness d with an inner surface of radius 100 cm. At any position d in the shield the dose equivalent due to the shower per initial photon resulting from the electromagnetic cascade was added to that due to the primary photons that have not been removed from the shield by exponential attenuation according to the value of $\langle \lambda_\gamma \rangle$. Thus, the electromagnetic component of the dose equivalent, $H_\gamma(d)$ was determined. Maximal values of neutron dose equivalent due to photoneutron reactions were calculated following Swanson (1979). Nowhere did the neutron dose equivalent amount to more than about one per cent of the total dose equivalent and was thus neglected.

Shielding of the hadronic component

The calculation of the hadronic component of the radiation field must include the attenuation of the initial charged pions by pion-nucleus interactions along with the resultant generation of secondary particles in a hadronic cascade. The loss of energy of the particles by ionization is also very important in this energy domain.

Fasso et al. (1990) provides a recipe for calculating the necessary pion-nucleus cross sections in a shielding material for laboratory kinetic energies above 50 MeV. In this formalism, the inelastic cross section in a collision of a hadron, h , with a nucleus of mass number A , σ_{inel}^{hA} , is given by

$$\sigma_{inel}^{hA} = \sigma_o A^\alpha. \quad (8)$$

Here σ_o and α are parameters determined from

$$\sigma_o = a + b\sigma_{tot}^{hp}, \text{ and} \quad (9)$$

$$\alpha = c - d\sigma_{tot}^{hp} \text{ or } \alpha = 2/3 \text{ if } c - d\sigma_{tot}^{hp} > 2/3. \quad (10)$$

σ_{tot}^{hp} is the total hadron-proton cross section and a , b , c , and d are particle-specific parameters. For both π^+ and π^- , $a = 5.0 \times 10^{-27} \text{ cm}^2$ and $d = 3.0 \times 10^{24} \text{ cm}^{-2}$. The dimensionless parameters b and c have the values 0.889 and 0.83, respectively. The values of σ_{tot}^{hp} were taken from Groom et al. (2000). In the relevant energy region, the values of σ_{tot}^{hp} for π^+ -proton collisions differ considerably from those for π^- -proton collisions. To determine values of $\sigma_{inel}^{\pi A}$, the values of $\sigma_{tot}^{\pi p}$ for π^+ and π^- were averaged. These cross sections were converted into mean free paths, λ_π , for each material, with the results shown in Fig. 4.

The charged pions will be stopped by ionization in reasonable thicknesses of

representative shielding materials. Values of the ionization range, R , for charged pions were taken from the tables of Barkas and Berger (1964). To illustrate the importance of both nuclear interactions and range-out (stopping by ionization), the average mean free path, $\langle \lambda_{\pi}(E_{\pi}) \rangle$ (cm), between a given value of charged pion kinetic energy, E_{π} , and zero kinetic energy was calculated and used to determine the probability that a given charged pion experiences a nuclear interaction prior to rangeout by evaluating the quantity $[1 - \exp(-R/\langle \lambda_{\pi}(E_{\pi}) \rangle)]$. The results are plotted along with the charged pion ranges in Fig. 5. Clearly, for the relevant energy region, both removal mechanisms are important. To address ionization, it was found that a simple power law provides an adequate fit to the range energy relation;

$$R = AE_{\pi}^B. \quad (11)$$

The values of fitting parameters are given in Table 3. If one considers a charged pion of initial kinetic energy, E_{π} , one can invert this equation to approximate the energy E'_{π} it retains following the penetration of a depth d of material;

$$E'_{\pi} = \left[\frac{AE_{\pi}^B - d}{A} \right]^{\frac{1}{B}}. \quad (12)$$

For those charged pions that experience inelastic collisions, one must consider the type and multiplicity of particles emergent from each interaction. While data are relatively scarce, Fasso et al. (1990) and Hänßgen (1987) provide some results. In the energy domain of interest, pion-nucleus multiplicities are similar in magnitude and energy dependence to proton-nucleus multiplicities with the singular qualitative difference that for the pion interactions, secondary charged pions tend to replace neutrons as the most prominent hadrons. Sullivan (1992) has

provided a formula that adequately describes the multiplicity, M , of secondary particles per interaction for protons of less than 1 GeV as a function of energy, E (MeV);

$$M(E) = 0.077E^{0.63}. \quad (13)$$

One can proceed to calculate the propagation of the radiation field through a material shield. The Bose-Einstein charged pion spectrum emerging from a point source was divided into bins of 10 MeV width. At given depth in the shield d , for each bin the energy remaining to the charged pion, E'_π was calculated using eqn (12). The average of the initial energy E_π and E'_π , eqn (13) was used to determine the average multiplicity of secondaries within the distance d assuming the original particle interacted. The probability of occurrence of an inelastic collision was determined using the value of $\langle \lambda_\pi(E_\pi) \rangle$. One can approximate the mean number of such interactions, n_{int} , that would occur in distance d ;

$$n_{\text{int}} = \frac{d}{\langle \lambda_\pi(E_\pi) \rangle}. \quad (14)$$

Thus, after depth, d , a simple buildup factor, $F_\pi(E_\pi, d)$ was calculated taking into account the probability of primary pion participation in an inelastic collision, and using the average energy in the thickness d ;

$$F_\pi(E_\pi, d) = 1 + \left\{ 1 - \exp\left(\frac{d}{\langle \lambda_\pi(E_\pi) \rangle}\right) \right\} \left\{ M\left(\frac{E_\pi + E'_\pi}{2}\right) \right\}^{n_{\text{int}}}. \quad (15)$$

This buildup factor is akin to that used by Lindenbaum (1961). It is an approximation because of the averaging which has been done and the factorization of the single probability of interaction rather than the performance of n_{int} integrations over the individual interactions. It will slightly overestimate the number of secondaries due to the lack of consideration of the energy dependence of their multiplicity for all generations beyond the first.

As with the electromagnetic component, calculations were performed for a point source surrounded by a spherical shield of thickness d having an inner surface of radius 100 cm. For each 10 MeV slice of the spectrum, the charged pion fluence was multiplied by $F_\pi(E_\pi, d)$ to determine the total hadron fluence. The total fluence was attenuated exponentially with $\langle\lambda_\pi(E_\pi)\rangle$ as the mean free path. Application of the dose equivalent per fluence conversion factor, $P_\pi(E_\pi)$ determined the dose equivalent. The very weak energy-dependence of this factor provides a significant simplification. Since this factor for charged pions is actually larger than that found for neutrons and comparable to that for protons of similar energies (Fasso et al. 1990), this choice is conservative. The results were then integrated over the entire spectrum. The integration, though performed numerically, is represented by

$$H_\pi(d) = \frac{\int_{E_{\min}}^{938} dE_\pi P_\pi(E_\pi) N_\pi(E_\pi) F_\pi(E_\pi, d) \left\{ 1 - \exp\left(-\frac{d}{\langle\lambda_\pi(E_\pi)\rangle}\right) \right\}}{4\pi r^2}, \quad (16)$$

where E_{\min} is the lowest energy at which d does not exceed the range of the primary pions. This lower limit of integration enforces the disappearance of incident pions by rangeout.

RESULTS

Figs. 6, 7, and 8 provide the results of these calculations for the six materials studied. In these figures, the effect of arbitrary choice of 100 cm for the inner radius has been removed by plotting the quantities $r^2 H(d)$ for both components of the radiation field and for the total dose equivalent. For each pair of materials, two plots are provided to better show details over all values of d studied, due to the much shorter scaling length of the electromagnetic component. In these figures, for the smaller values of d , one can clearly see the buildup of the electromagnetic

cascades, especially in the materials of higher atomic number. The sub-exponential falloff with energy of the curves for the hadronic component reflects the importance of range-out.

DISCUSSION

The results provided a basis for estimating the prompt radiation hazards of stored antiprotons. A few examples illustrate the level of hazard. Discounting any self-shielding of a Penning trap used to transport stored antiprotons, at $r = 100$ cm, $H_\gamma = 6.17 \times 10^{-15}$ Sv per annihilation while $H_\pi = 3.93 \times 10^{-14}$ Sv per annihilation for a total of 4.55×10^{-14} Sv per annihilation for a “bare” source. Thus, if 10^{12} antiprotons are stored and annihilate in a failure of the trap, the dose equivalent at this distance would be 4.6×10^{-2} Sv (4.6 rem). For, say, 10^9 stored antiprotons, the dose equivalent at $r = 100$ cm of $46 \mu\text{Sv}$ (4.6 mrem) for an unshield source is, arguably, trivial for infrequent events.

From Fig. 8, a concrete shield of 50 cm thickness reduces the value of r^2H to 1.2×10^{-10} Sv cm^2 per annihilation. If this shield begins at a radial distance of, say, 50 cm, then for 10^{12} stored antiprotons, the total dose equivalent in such an accident is estimated to be about 0.012 Sv (1.2 rem). However, if a lead shield is chosen of this same thickness, r^2H is 1.7×10^{-11} Sv per annihilation in such an accident involving 10^{12} stored antiprotons so that the dose equivalent is 1.7×10^{-3} Sv (0.17 rem), a much more manageable situation. For iron, the same thickness of shield at the same radius would present a dose equivalent of 2.4×10^{-3} Sv (0.24 rem). For lead, copper, and iron, another order of magnitude of reduction is possible for modest increments of shielding material. For any of these shields, especially for large numbers of antiprotons, it is advisable to incorporate a thin (≈ 1 -2 cm) outer layer of hydrogenous material, or borated hydrogenous materials such as borated polyethylene to dispose of very low energy neutrons not

considered in detail in the present calculation. It is rather clear that the higher density materials, as expected, are more efficient shields

CONCLUSION

The radiation fields produced by antiproton-nucleon annihilations at rest have been described in a simple picture. It is clear that when large quantities of antiprotons are stored, the radiological hazards must be addressed. For small quantities, the prompt radiation hazards are negligible. Standard shielding techniques can mitigate the hazard of the sudden loss of the antiprotons. Since these prompt radiation hazards are somewhat novel, the regulatory paradigm concerning transport and use of storage devices for these particles differs from the usual considerations that pertain to radioactive materials shipments or, for that matter, to other types of radiological activities and will require further discussion. The results in this paper may be useful in addressing these questions. Future work for actual installations should employ more sophisticated shielding calculations than the illustrations performed here in order to properly reflect the details of a particular configuration.

Acknowledgments-The author has benefited greatly from helpful comments received from Drs. Alexander Elwyn and Kamran Vaziri. This work was supported by the U. S. Department of Energy under Contract No. DE-AC02-76CH03000.

REFERENCES

- Amsler C, Myhrer F. Low energy antiproton physics. *Ann Rev Nucl Part Sci* 41:219-267; 1991.
- Amsler C. Proton-antiproton annihilation and meson spectroscopy with the Crystal Barrel. *Rev Mod Phys* 70:1293-1339; (1998).
- Angelopoulos A, et al. Study of charged particle production in $p\bar{p}$ annihilations at rest. In: Antiproton 86 VII European symposium on nucleon-antinucleon interactions. Charalambous S, Papastefanou C, Pavlopoulos P. eds. Singapore: World Scientific; 1986: 79-204.
- Barkas WH and Berger MJ, Tables of energy losses and ranges of heavy charged particles. Report NASA-SP-3013. Washington: National Aeronautics and Space Administration; 1964.
- Berger MJ, Seltzer SM, Tables of energy losses and ranges of electrons and positrons, Report NASA-SP-3012. Washington: National Aeronautics and Space Administration; 1964.
- Berger MJ, Hubbell JH, Seltzer SM, Coursey, Zucker DS. XCOM: photon cross section database, NIST standard reference 8 (XGAM). National Institute of Standards and Technology, U.S. Department of Commerce; 2002. Available at <http://physics.nist.gov/PhysRefData/Xcom/Text/Xcom.html>.
- Brown LS, Gabrielse G. Geonium theory: Physics of a single electron or ion in a Penning trap. *Rev Mod Phys* 58: 233-311; 1986.
- Chilton AB, Shultis JK, Faw RE. Principles of radiation shielding. Englewood Cliffs, NJ: Prentice-Hall, Inc; 1984.
- Eades J, Hartmann FJ. Forty years of antiprotons. *Rev Mod Phys* 71: 373-419; 1999.
- Fasso A, Goebel K, Höfert M, Ranft J, Stevenson G. Shielding against high energy radiation.

- Vol 11 in Schopper H, ed. Vol 11 Landolt-Börnstein numerical data and functional relationships in science and technology, new series. Berlin: Springer Verlag; 1990.
- Gabrielse G, Fei X, Helmerson K, Rolston SL, Tjoelker R, Trainor TA, Kalinowsky H, Haas J, Kells W. First capture of antiprotons in a Penning trap: A kiloelectronvolt source. *Phys Rev Lett* 57: 2504-2507; 1986.
- Gabrielse G. Harvard University: Gabrielse Research Group; 2002. Available at: <http://hussle.harvard.edu/~gabrielse/>.
- Graf NA, et al. Search for narrow states in the inclusive γ -ray spectra resulting from antiproton annihilations at rest in liquid hydrogen and deuterium. *Phys Rev D* 44:1945-1961; 1991.
- Gregory P, Mason P, Muirhead H, Warren G, Hamer CJ, Ekspong G, Carlsson R, Holmgren SO, Nilsson S, Stenbacka R, Walk Ch. Search for single cluster formation in annihilation reactions. *Nucl Phys B* 102:189-206; 1976.
- Groom DE et al. Review of particle properties. *Eur Phys Jour C* 15:1-878; 2000. Available at: <http://pdg.lbl.gov/>.
- Hänßgen K. Hadronic event generation for hadron cascade calculations and detector simulation- Part IV; The application of the intranuclear cascade model to reactions of pions, nucleons, kaons, and their antiparticles with nuclei below 6 GeV/c. *Nucl Sci Eng* 95:135-147; 1987.
- Howe SD, Hynes MV, Picklesimer A. Portable pbars, traps that travel. In: Antiproton science and technology. Proceedings of a RAND workshop, Santa Monica, CA, 6-9 October 1987. Singapore: World Scientific; 1988: 481-481. (Also available as Los Alamos National Laboratory Report LA-UR-88-737; 1988).
- Landau R. Meson spectroscopy at LEAR. *Ann Rev Nucl Part Sci* 46:351-393; 1996.

Lindenbaum SJ. Shielding of high energy accelerators. *Ann Rev Nucl Sci* 11:213-258; 1961.

Pais A. The many π -meson problem. *Ann of Phys.* 9:548-602; 1960.

Rossi B, Griegen K. Cosmic-ray theory. *Rev Mod Phys* 13:240-309; 1941.

Stevenson GR. Dose equivalent per star in hadronic cascade calculations, European Organization for Nuclear Research (CERN): CERN Divisional Report TIS-RP/173; 1986.

Sullivan AH. A guide to radiation and radioactivity levels near high energy particle accelerators. Ashford, Kent, England: Nuclear Technology Publishing; 1992.

Swanson WP. Radiological safety aspects of the operation of electron linear colliders. Technical Report Series No. 188. Vienna: International Atomic Energy Agency; 1979.

Tolman RC. The principles of statistical mechanics. London: Oxford University Press; 1938.

Tseng CH, Gabrielse G. Portable trap carries particles 5000 kilometers. *Hyperfine Inter* 76: 381-386; 1993.

FOOTNOTE

[†]While the two values of kT were arbitrarily used to fit the spectra to the calculated average energies of photons and charged pions, their magnitudes are sensible if one naively assumes that the proton and antiproton overlap immediately prior to annihilation and that each of the five pions are localized within one fifth of a spherical volume having a 1.2 fm radius, a representative nucleon "size", immediately prior to the annihilation. Application of the Heisenberg uncertainty principle results in a momentum of 206 MeV/c and a kinetic energy of 108 MeV.

Table 1 Material-dependent properties used in shielding calculations

Material	ρ (g cm ⁻³)	X_o (g cm ⁻²)	E_{crit} (MeV)
Carbon	2.27	42.69	81.65
Aluminum	2.70	24.01	42.70
Iron	7.87	13.84	21.68
Copper	8.96	12.86	19.41
Lead	11.35	6.37	7.43
Concrete	2.40	26.54	49.74

Table 2 Parameters associated with calculations of the radiative part of the electromagnetic component

Material	$\langle\lambda_\gamma\rangle$ (g cm ⁻²)	F_{pair}	F_{shower}	F_{em}	$\langle d_{shower}\rangle$ (cm)	τ (cm)	D_{max} (MeV- cm ² g ⁻¹)	C_{mat} (Sv Gy ⁻¹)
Carbon	65.83	0.84	0.28	0.24	6.16	28.1	0.40	1.0 ^a
Aluminum	38.24	0.91	0.42	0.38	8.73	16.1	0.81	1.2
Iron	22.30	0.94	0.57	0.54	2.93	3.67	1.59	1.3
Copper	20.76	0.95	0.58	0.55	2.55	3.06	1.71	1.3 ^a
Lead	10.45	0.98	0.75	0.73	1.54	1.38	3.78	1.8
Concrete	40.61	0.90	0.40	0.36	9.15	19.2	0.73	1.2

^aValues estimated from others provided by Fasso et al. (1990).

Table 3 Parameters used in the power law fit of the range-energy relation for charged pion kinetic energies in MeV

Material	A (cm)	B	Coefficient of Correlation
Carbon	2.5771×10^{-2}	1.3419	0.99621
Aluminum	2.5857×10^{-2}	1.3291	0.99615
Iron	1.0115×10^{-2}	1.3227	0.99613
Copper	9.3544×10^{-3}	1.3197	0.99614
Lead	1.1176×10^{-2}	1.2917	0.99604
Concrete	2.7033×10^{-2}	1.3346	0.99618

List of Figure Captions

1. Normalized Bose-Einstein photon energy spectrum, referenced Monte Carlo spectrum of Graf et al. (1991), and dose equivalent per unit fluence conversion factors, $P_\gamma(E_\gamma)$, described in the text plotted as a function of photon energy.
2. Normalized Bose-Einstein charged pion spectrum along with the Measured Spectrum 1 of Gregory et al. (1976) and Measured Spectrum 2 of Angelopoulos et al. (1986) as well as the dose equivalent per unit fluence factors for charged pions, $P_\pi(E_\pi)$, described in the text plotted as a function of charged pion kinetic energy. The normalizations of the measured spectra are arbitrary.
3. Photon mean free paths for various materials plotted as a function of photon energy taken from the database of Berger et al. (2002). All physical effects are included. The symbols appearing on each curve are intended to guide the eye.
4. Plot of charged pion mean free paths in various materials plotted as a function of pion energy calculated as described in the text. The symbols appearing on each curve are intended to guide the eye.
5. Plot of the probability of nuclear interaction prior to rangeout (left ordinate) and ionization range (right ordinate) as a function of charged pion energy (abscissa). The symbols appearing on each curve are intended to guide the eye.
6. Plots of the product Hr^2 for carbon and iron. The contributions due to the electromagnetic (π^0 's) and hadronic (π^\pm 's) components of the radiation field as well as the total are shown. The upper frame is intended to show details at small values of d . The symbols on the curves are intended to guide the eye.
7. Plots of the product Hr^2 for aluminum and copper. The contributions due to the

electromagnetic (π^0 's) and hadronic (π^\pm 's) components of the radiation field as well as the total are shown. The upper frame is intended to show details at small values of d . The symbols on the curves are intended to guide the eye.

8. Plots of the product Hr^2 for concrete and lead. The contributions due to the electromagnetic (π^0 's) and hadronic (π^\pm 's) components of the radiation field as well as the total are shown. The upper frame is intended to show details at small values of d . The symbols on the curves are intended to guide the eye.

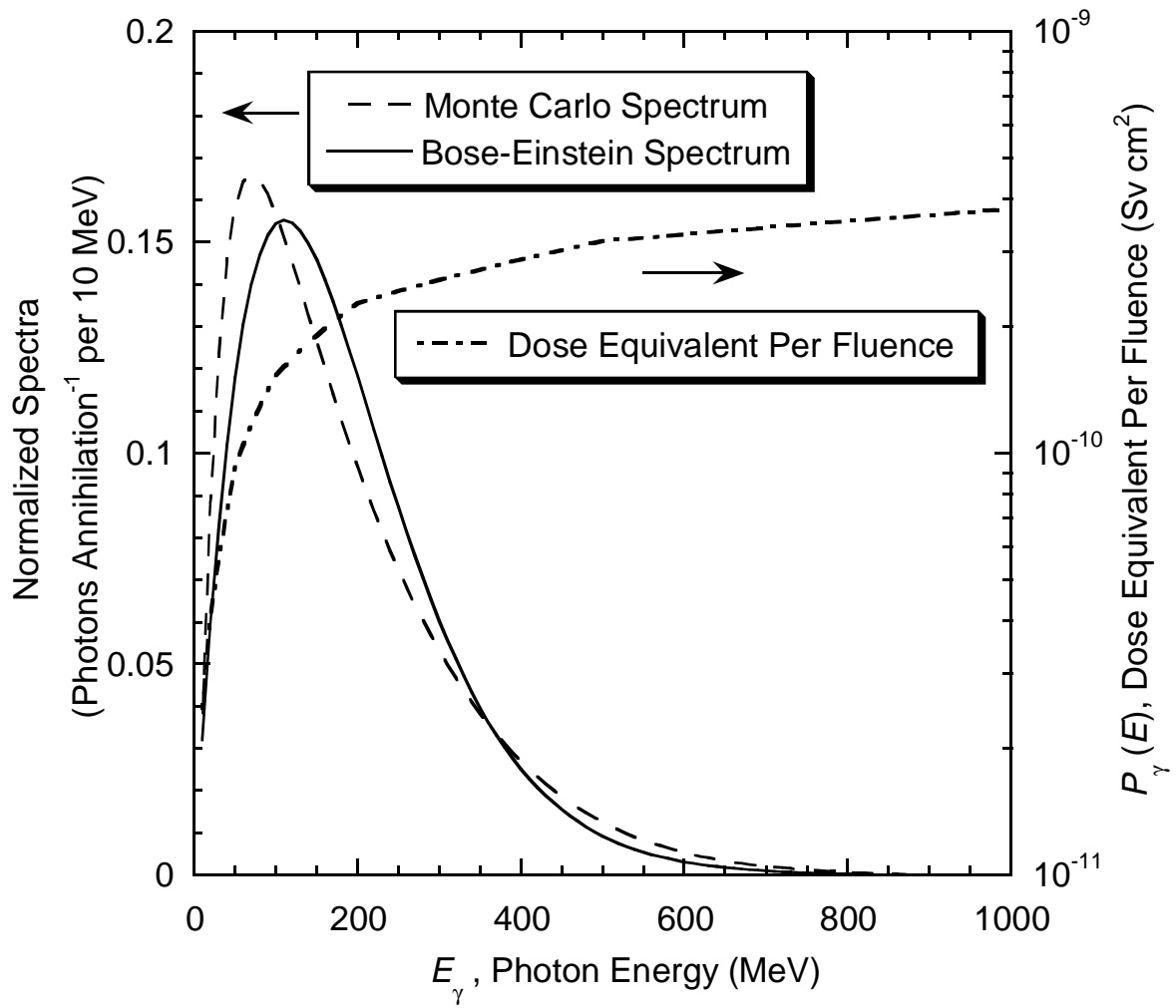


Figure 1

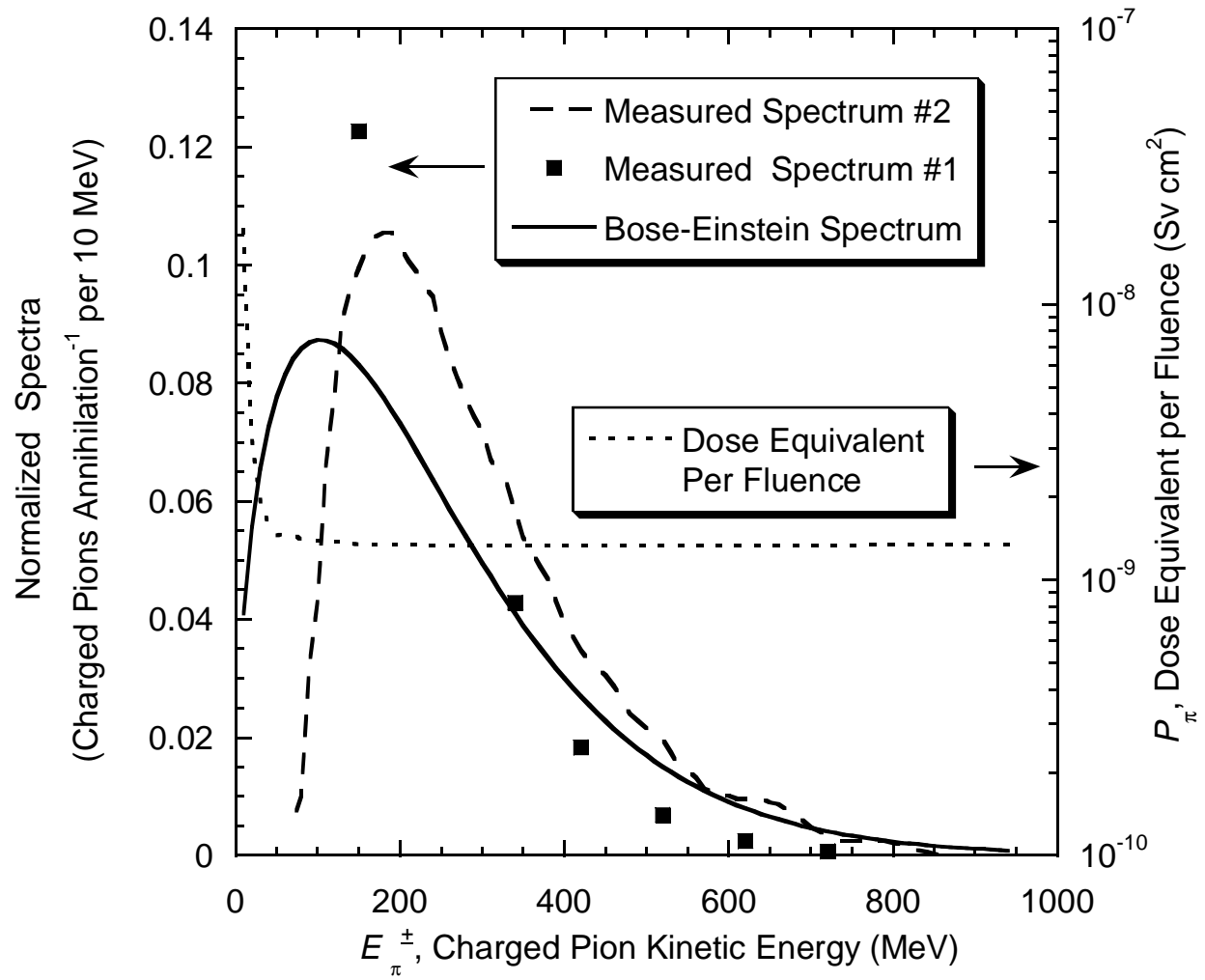


Figure 2

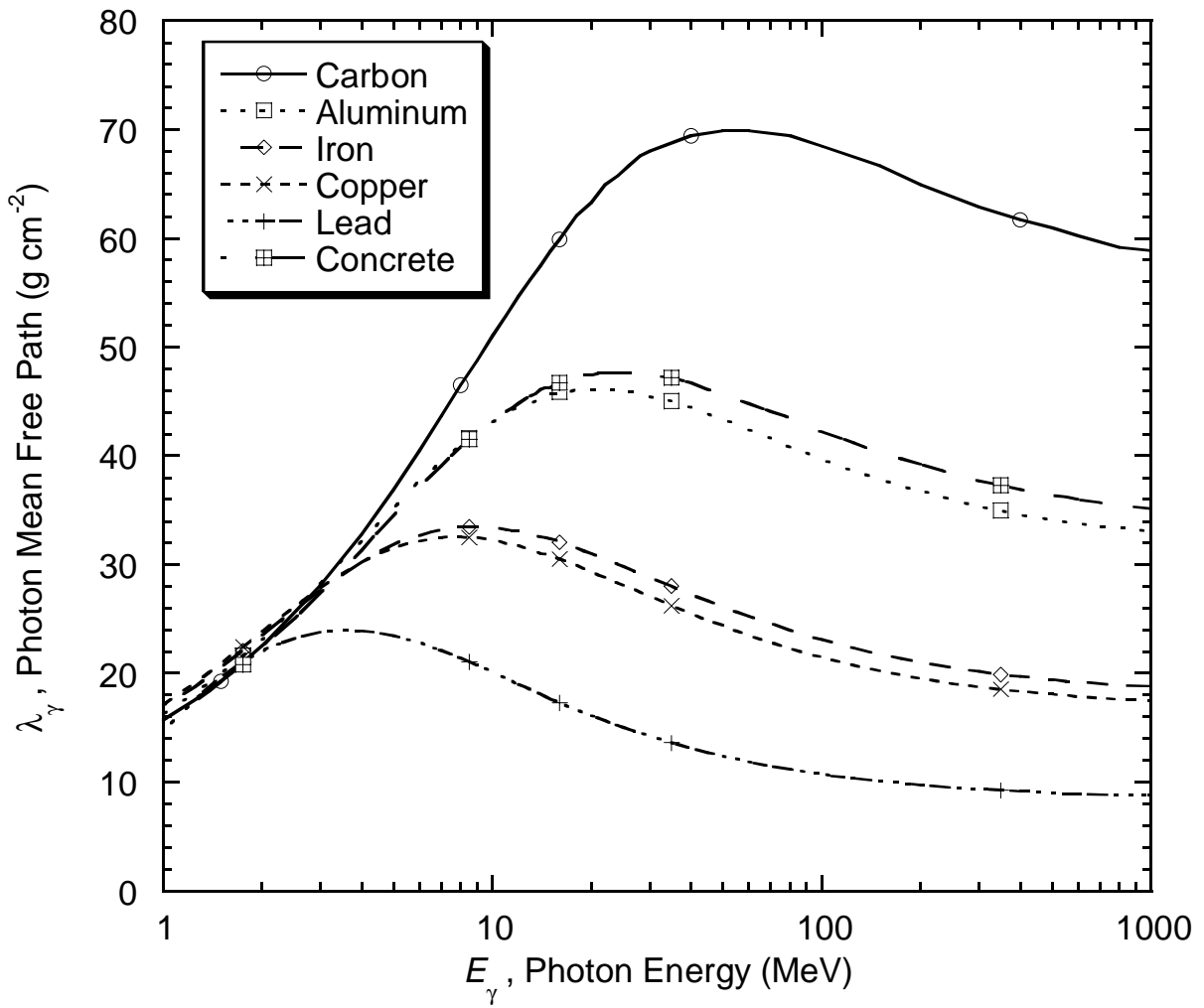


Figure 3

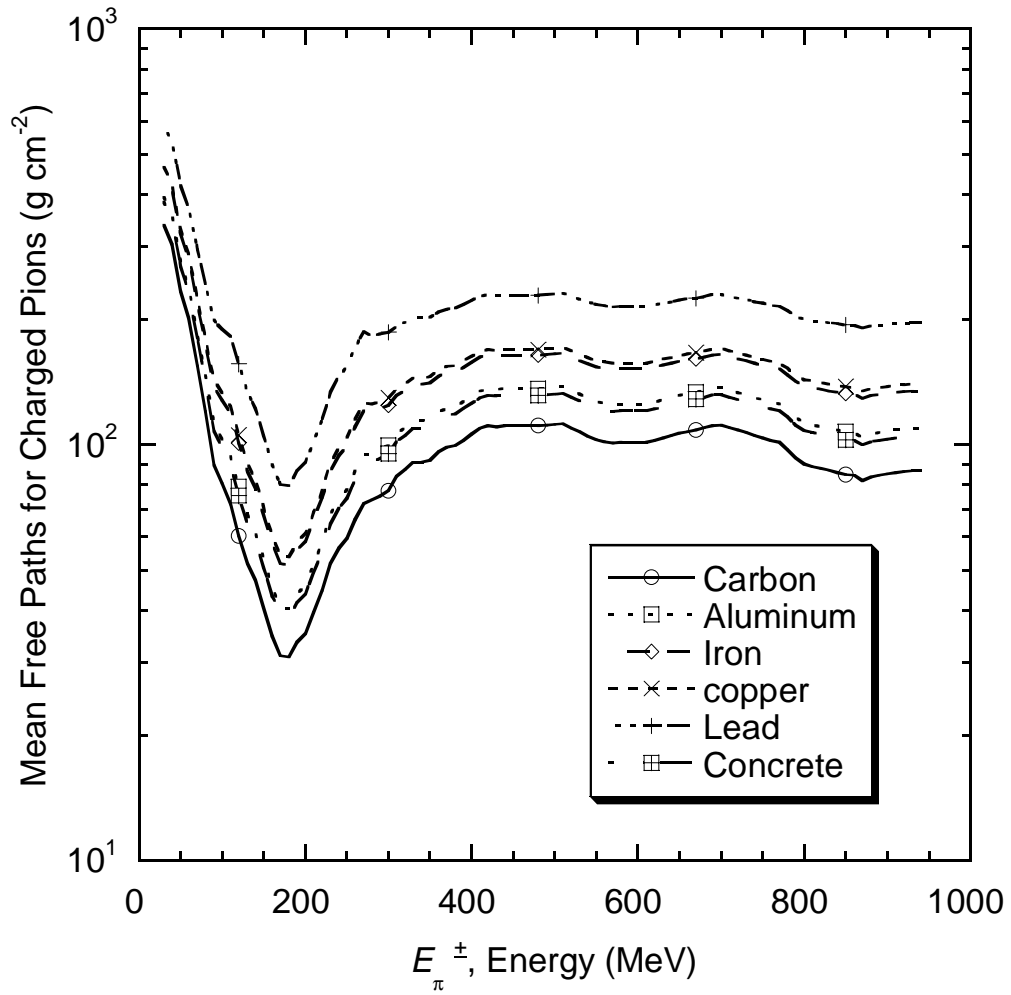


Figure 4

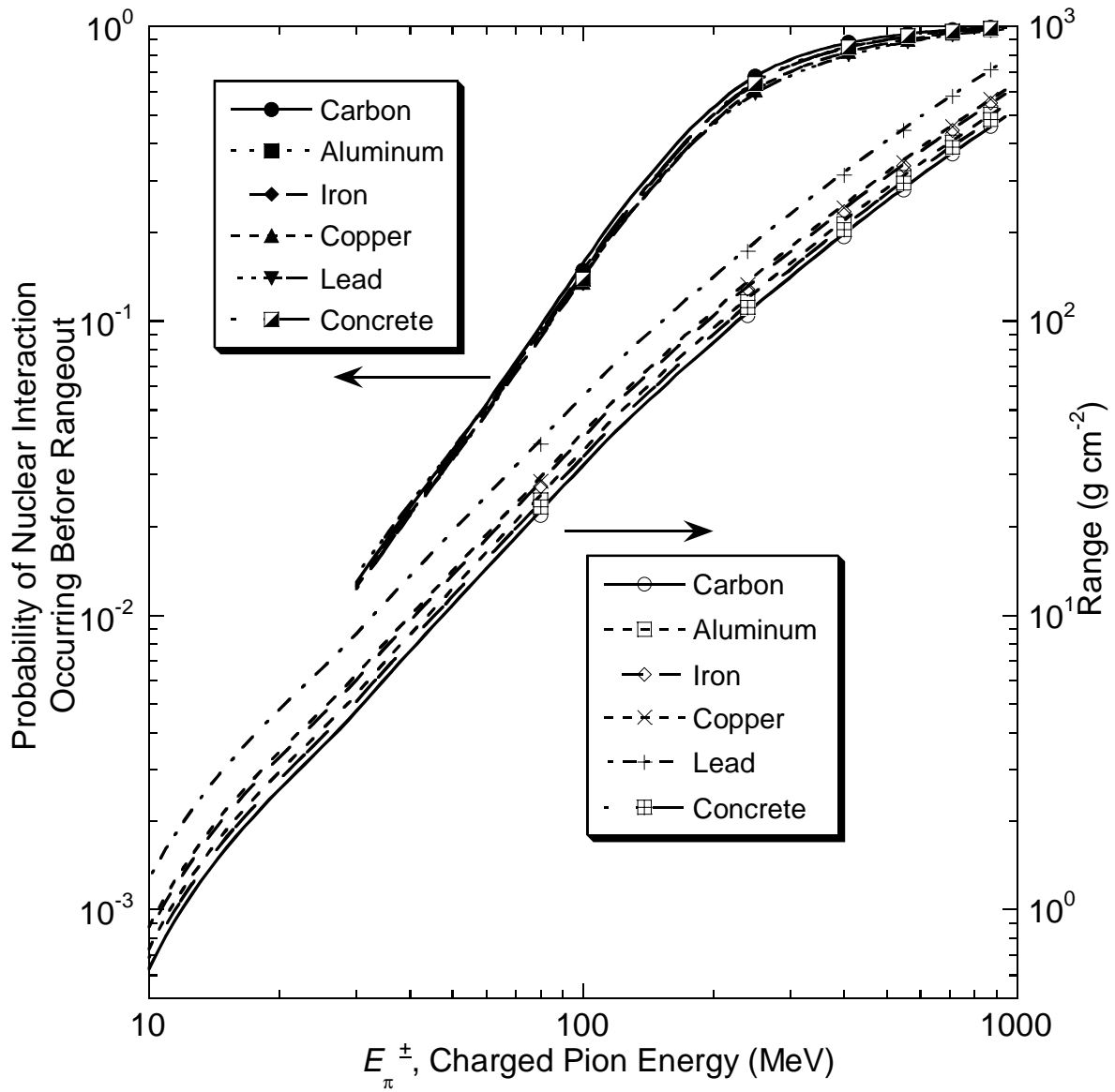


Figure 5

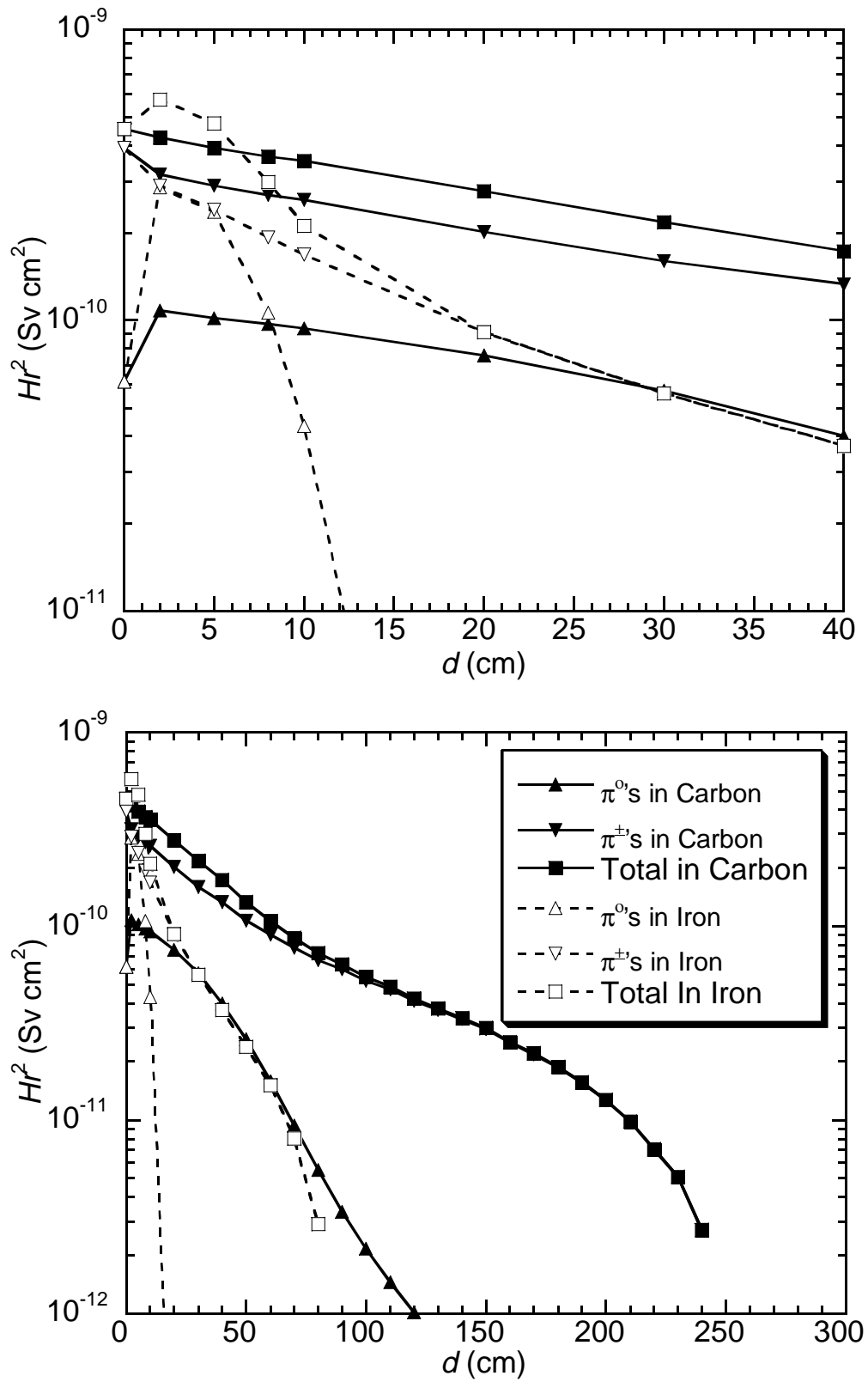


Figure 6

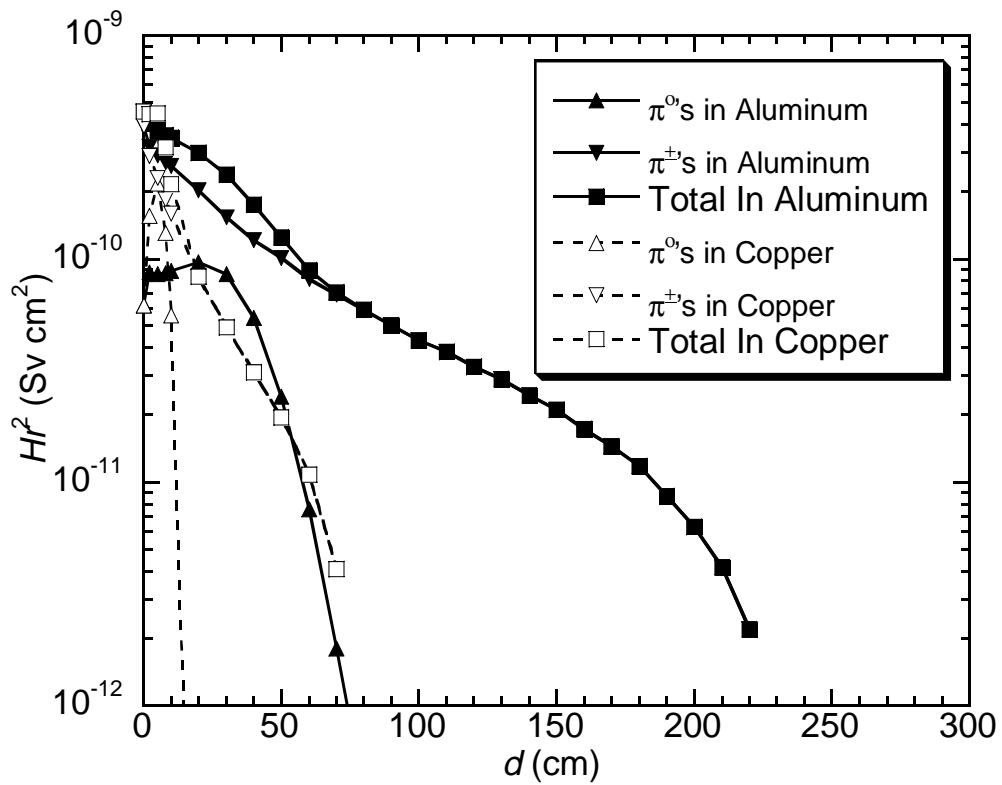
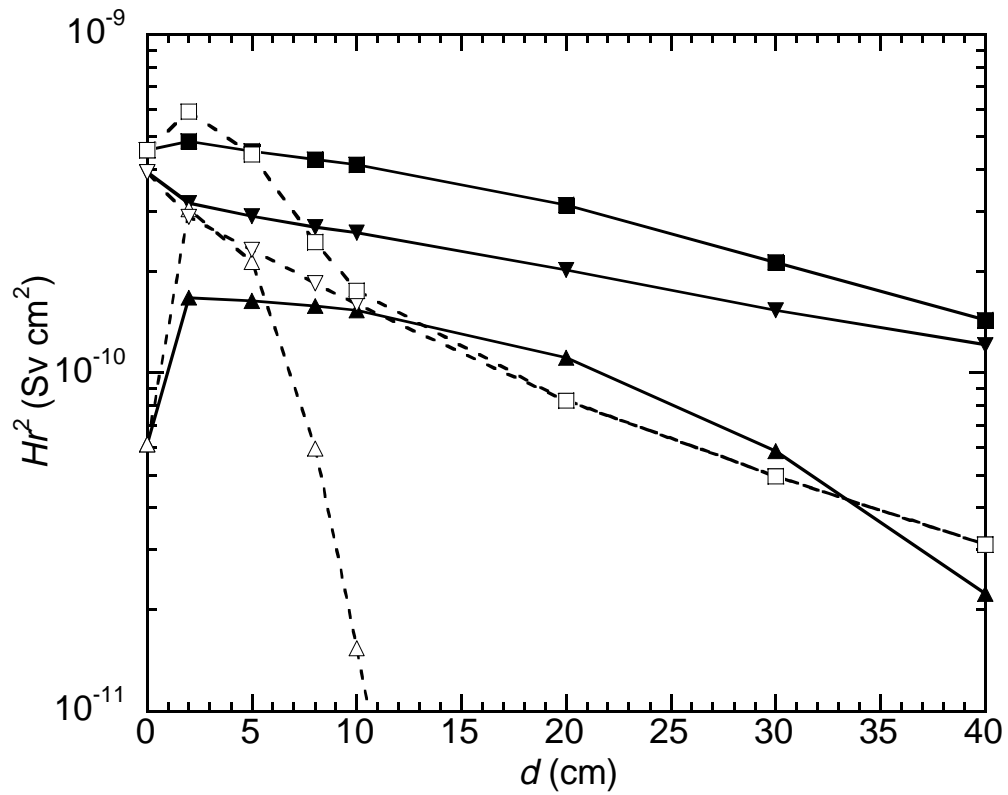


Figure 7

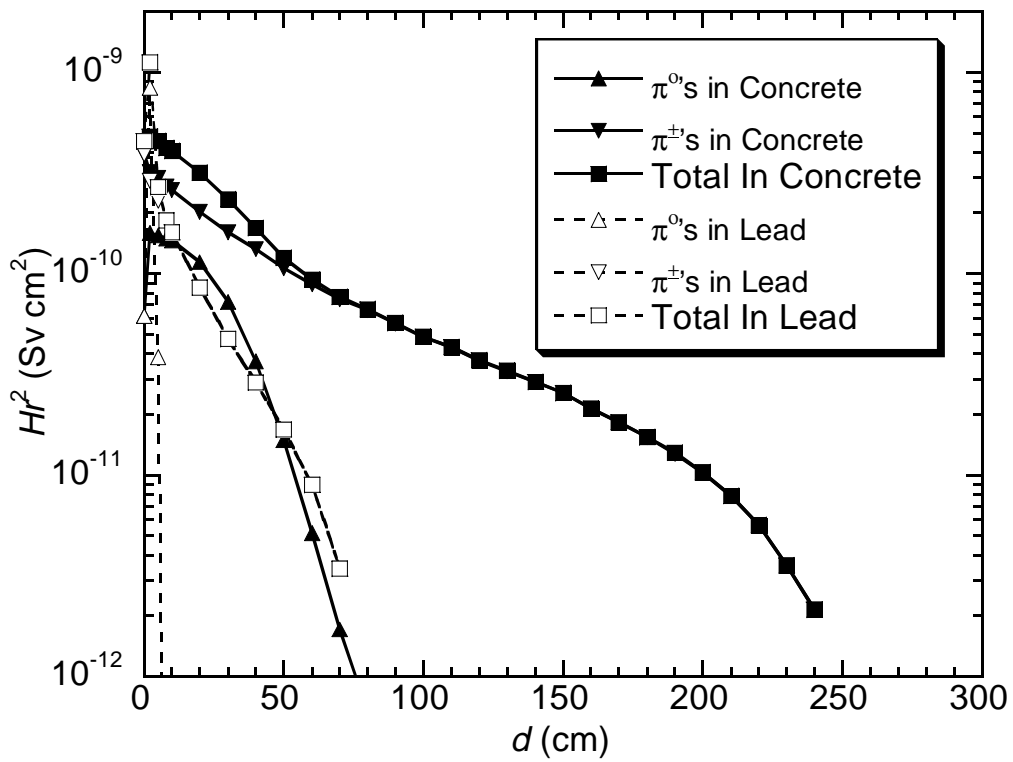
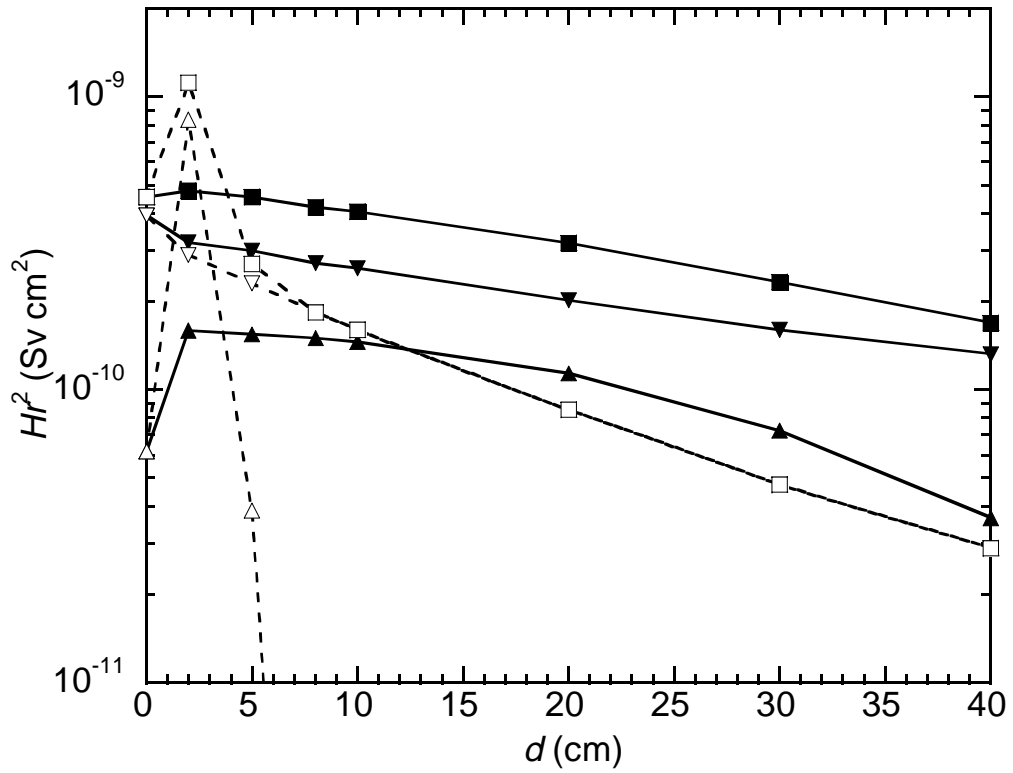


Figure 8